Direct Visualization of Single-Molecule Translocations through Synthetic Nanopores Comparable in Size to a Molecule

Volker Kurz, Edward M. Nelson, Jiwook Shim, and Gregory Timp*

Departments of Electrical Engineering and Biological Science, University of Notre Dame, Notre Dame, Indiana 46556, United States

ABSTRACT A nanopore is the ultimate analytical tool. It can be used to detect DNA, RNA, oligonucleotides, and proteins with submolecular sensitivity. This extreme sensitivity is derived from the electric signal associated with the occlusion that develops during the translocation of the analyte across a membrane through a pore immersed in electrolyte. A larger occluded volume results in an improvement in the signal-to-noise ratio, and so the pore geometry should be made comparable to the size of the target molecule. However, the pore geometry also affects the electric field, the charge density, the electro-osmotic flow, the capture volume, and the response time. Seeking an optimal pore geometry, we tracked the molecular motion in three dimensions with high resolution, visualizing with confocal microscopy the fluorescence associated with DNA translocating through nanopores with diameters comparable to the double helix, while simultaneously measuring the pore current. Measurements reveal single molecules translocating across the membrane through the pore commensurate with the observation of a current blockade. To explain the motion of the molecule near the pore, finite-element simulations were employed that account for diffusion, electrophoresis, and the electro-osmotic flow. According to this analysis, detection using a nanopore comparable in diameter to the double helix represents a compromise between sensitivity, capture volume, the minimum detectable concentration, and response time.

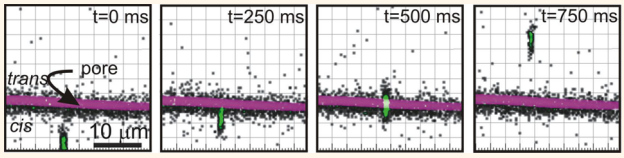

KEYWORDS: nanopore · single molecule · DNA · fluorescence · electro-osmotic flow

A nanopore can be used to analyze a molecule with submolecular sensitivity, provided the diameter is small enough.[1−4] Cutting-edge applications of nanopore technology range from sequencing DNA[1−5] to scrutinizing the structure of a protein as the molecule unfolds.[6−9] This extreme single-molecule sensitivity is derived from the electric signal associated with the occlusion that develops when an analyte translocates across a membrane through a pore immersed in electrolyte. A larger occluded volume results in an improvement in the signal-to-noise ratio associated with a blockade in the electrolytic current through the pore. Thus, the pore geometry is the key to its utility; it affects the electric field, the charge density, the electro-osmotic flow, the capture radius, and the response time.

Due to the fragility of proteinaceous pores in a lipid layer[10] and the challenges presented by an *ab initio* protein design,[11,12] recent efforts in single-molecule detection have focused on nanopores in solid-state membranes, but this work suffers from ambiguities in the interpretation of the electrical signature of a molecule. For example, a current blockade associated with the occluded electrolytic current through the nanopore can develop even if the molecule is not in the pore lumen;[13] it is possible to observe current enhancements above the open pore current as well as blockades associated with the translocation of the same nucleic acid through the same pore,[13] depending on the electrolyte molarity[14,15] and molecular configuration;[16] the deepest blockades are not always indicative of a translocation across the membrane;[17,18] and transient collisions of the analyte with the pore entrance may occur that give rise to a blockade without a translocation.[6,19−21]

To inform on the relationship between the molecular motion and configuration, and the current transients and occluded

* Address correspondence to gtimp@nd.edu.

Received for review January 13, 2013 and accepted April 22, 2013.

Published online April 22, 2013
10.1021/nn400182s

electrolytic volume, single-molecule fluorescence has been measured simultaneously with the pore current.[22−27] Early work that correlated fluorescent and current measurements through α-hemolysin proteins embedded in lipid membranes showed that the electrolytic current is directly related to the transport of Ca^{2+} ions through a single pore.[24] More recent efforts focused on nanopores comparable to the size of the molecule in solid-state membranes but lacked sufficient spatial resolution to track the motion of DNA as it translocated through the pore[25] or to deduce the molecular configuration. Measurements with high spatial resolution have been limited to pores with diameters >50 nm, much larger than the size of a molecule[23,26] or pores much longer ~20 μm than the molecule.[27] Taken altogether, prior work does not establish the relation between the current through a nanopore comparable in size to the molecule and the three-dimensional (3D) molecular motion through it with sufficient resolution. Yet, a nanopore with a diameter comparable in size to the molecule remains the primary focus due to the potential for improving the signal-to-noise ratio.

Seeking the optimal pore geometry, we tracked the molecular motion in 3D with high resolution, visualizing with confocal microscopy the fluorescence associated with double-stranded linear and circular DNA (dsDNA) translocating through nanopores with diameters comparable to the double helix, while simultaneously measuring the pore current. The measurements were performed on nanopores in silicon nitride membranes embedded in a transparent microfluidic device that allowed fluidic, electrical, and optical access all at the same time. The microfluidic device was anchored to a high-speed piezo-scanner on a confocal microscope for high-resolution 3D imaging. To facilitate high-speed fluorescence measurements commensurate with the duration of a current blockade without photobleaching, the weak DNA autofluorescence was augmented by intercalation with a fluorophore, YOYO-1. While it has been shown that fluorophores intercalated into molecules can be impelled through a pore with a only subtle effect on the resulting current transients,[28] the fluorescence can be used to delineate the molecular position and configuration, provided it can be resolved.

Visualization of single-molecule fluorescence, performed simultaneously with nanopore current measurements on the most dilute concentrations of DNA reported so far, reveals single molecules translocating across the membrane through the pore commensurate with the observation of a current blockade, which is sometimes followed by an enhancement of the current above the open pore value, in correspondence with predictions.[13] However, even in the absence of a translocation, false positives in the current can be associated with molecules obstructing the pore but not translocating through it. To explain the motion of the molecules near the pore, we employed finite-element (FE) simulations that account for diffusion, electrophoresis, and the electro-osmotic flow. According to this analysis, single-molecule detection using a nanopore comparable in diameter to the double helix represents a compromise between sensitivity and capture volume.

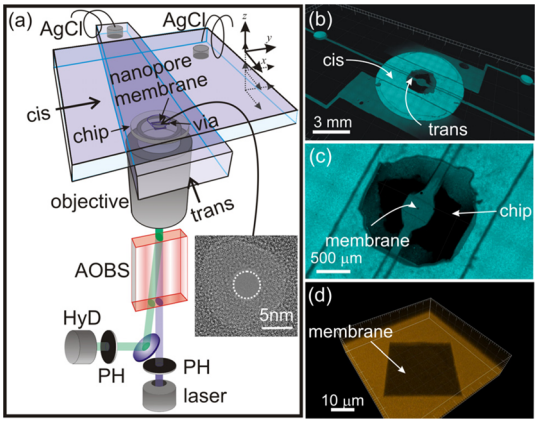

Figure 1. (a) Schematic of the confocal microscope with a two-layer microfluidic mounted on the stage. This instrument uses conjugate focal planes: the objective lens of the confocal is used to both excite with an argon laser and collect the fluorescent light emitted by the DNA through pinholes. An acousto-optic beam splitter (AOBS) deflects the fluorescence light into a HyD detector. A microfluidic is mounted on the piezo-stage that allows for translation with nanometer-scale precision along the *x*, *y*, or *z* axes. A silicon chip that supports a thin silicon nitride membrane with a nanopore in it is embedded in the microfluidic. The nanopore spans the membrane, connecting the *cis*- and *trans*-chambers of the microfluidic. The inset shows a TEM of a (3.5 × 4.1) ± 0.2 nm cross section pore sputtered in a silicon nitride membrane 30 ± 2.0 nm thick. (b) Concatenated confocal images of the microfluidic obtained at low magnification (10×) showing the *cis*- and *trans*-chambers. (c) Magnification of the confocal data set in (b) showing the silicon chip and the 30 μm SiN membrane. (d) Confocal image of the silicon nitride membrane.

RESULTS AND DISCUSSION

Nanopores with a cross section comparable to the DNA double helix or the bending radius of a circular plasmid are at the crux of this work. A TEM image of a typical pore with a (3.5 × 4.1) ± 0.2 nm cross section in a silicon nitride membrane 30 ± 2 nm thick is shown in the inset to Figure 1a. A nanopore is created by sputtering through a silicon nitride membrane <30 nm thick on a silicon handle wafer using a high-energy (300 kV), tightly focused electron beam (see Methods). Subsequently, the chip supporting the membrane is plasma bonded to a multilevel microfluidic device that seals the chip to the microfluidic device between the two *vias*, leaving the pore as the only connection between the *cis*- and *trans*-channels, as illustrated in Figure 1a−c.[29,30] From TEM images taken at different tilt angles, it was inferred that the pore geometry is biconical, each with <20° cone angle.[29] The biconical

pore geometry combined with the surface charge in the pore has the benefit of focusing the electric field toward the center of the membrane—most of the voltage drop occurs over ~4.5 nm region near the constriction in the center of the membrane where the molecule is detected.[31]

We have previously established the distribution of the electrostatic potential in nanopores like these through measurements of the concentration dependence of the conductance and molecular dynamics (MD) simulations.[31] Moreover, it was also shown that the distribution of the electrostatic potential in a nanopore was roughly the same regardless of whether or not a nucleic acid was in the pore. However, MD does not account for the capture or exit of the molecule from the pore. In particular, it is naïve to suppose that the motion of the DNA is described simply by diffusion up to the orifice, where the electric force associated with an applied transmembrane potential finally impels the highly charged polyanion through the pore.[32] In addition to the electric field, there are other interactions affecting the net force on the DNA in and around the pore, which include the reduction of the driving force by the counterion condensation, the hydrodynamic drag of the electro-osmotic flow driven by the motion of counterions near the DNA and pore surface, the mechanical friction between DNA and the pore, and the hydrophobic adhesion of bases to the pore surface.[33,34]

Visualization of DNA Translocations. Fluorescence microscopy has been shown to be especially effective for visualizing long polymer chains in dilute solutions.[35−38] Provided the molecule is large enough to be resolved, it should also be possible to observe the (Brownian) motion of DNA and obtain information about the transport and conformation of individual molecules in solution with confocal fluorescence microscopy. However, dsDNA shows only a weak autofluorescence (the quantum yield is only 10^{-5}−10^{-4} with absorption in the range of 200−300 nm), and so to track the motion with fluorescence microscopy, the dsDNA was first intercalated with YOYO-1 iodide dye (Invitrogen) (see Methods). In particular, high-speed fluorescence imaging of a solution of DNA molecules was used to track the motion and estimate the diffusivity of single 20 kbp linear and 8.6 kbp circular plasmid dsDNA molecules. (Typical examples given in the movies S1a, b, which were acquired at 27 fps, are relegated to the Supporting Information.) To acquire the data, a $\lambda = 488$ nm wavelength laser beam was focused on the *cis*-side of the membrane, which contains fluorescent DNA in solution so dilute that there was not more than one molecule within the confocal volume. These images were subsequently analyzed using particle tracking algorithms that detect the particle's position by calculating the intensity-weighted mean position of pixels having a value above a certain threshold (see Methods). It was estimated that for a 10 pM concentration of DNA there is less than one molecule in the depth of focus; that is, only 1 molecule/$(5.5\ \mu\text{m})^3$ = 1/166 μm^{-3}, corresponding to the confocal volume of $\pi \times (1\ \mu\text{m})^2 \times 8\ \mu\text{m} = 25\ \mu\text{m}^3$. For normal 3D diffusion, it is expected that $D = \varepsilon^2/6\delta t$, where δt is the time between each frame and ε is the average distance the molecule moved. However, since only the $x-y$ projection of that motion was observed, the diffusivity is given by $D = \varepsilon^2/4\delta t$. As shown in Figure S1 in the Supporting Information, for a 4.5 pM concentration of dsDNA in 100 mM KCl, the diffusion coefficients above the membrane are $D = 1.573\ \mu\text{m}^2\ \text{s}^{-1}$ and $D = 2.238\ \mu\text{m}^2\ \text{s}^{-1}$ for linear (20 kbp) and circular (8.6 kbp) plasmids, respectively, so that in 290 ms it is expected that the molecule covers a distance of $L_d \approx (Dt)^{1/2}$ = 675 nm (L_d = 806 nm for circular plasmids) if diffusive transport predominates. This measurement of the DNA diffusion coefficient is consistent with prior work showing a topologically independent scaling law $D \sim L^{-\nu}$, where L is the molecular length, and $\nu_l = 0.571 \pm 0.014$ and $\nu_s = 0.571 \pm 0.57$ for linear and supercoiled circular plasmid DNA, respectively.[37] Our measurements show no evidence of photocleavage of the dsDNA since the experiment for the diffusion constant reveals only a single Gaussian distribution of distances between two frames signifying a unique size of the molecule.

The measurements described above were performed directly over the pore but in the absence of an electric field. To measure the effect of the electric field and electro-osmotic flow on transport, the motion of linear DNA was tracked near a nanopore with a transmembrane voltage applied. The timing of the data acquisition in these measurements represents a compromise between the extent of molecular motion in a field or flow, the depth of focus and scan area required to track the molecule and photobleaching. Ideally, to elucidate the relationship to the molecular configuration in a nanopore, the translocation velocity has to be made slower than the maximum scanner rate. Since the maximum scanning rate is 8 kHz, the minimum duration current transient must be longer than 125 μs. One approach pursued to slow the translocation velocity of linear DNA was to increase the friction by using a pore that is comparable in size to the double helix,[39,40] while at the same time decreasing the impelling force by reducing the effective charge by intercalating the molecule with YOYO-1. YOYO-1 carries four positive charges, which partially neutralizes the phosphate charge on the DNA backbone, reducing it by approximately a factor of 2 for this loading.[38] The mean dwell time was calculated by fitting a normal distribution to the logarithm of the event time. Choosing a 3.8 nm diameter pore in a 30 nm thick membrane, our measurements reveal an average dwell time in the pore of only $t_D \sim 589 \pm 28\ \mu$s at a 1 V transmembrane bias, corresponding to a translocation velocity of ~1.13 cm/s,

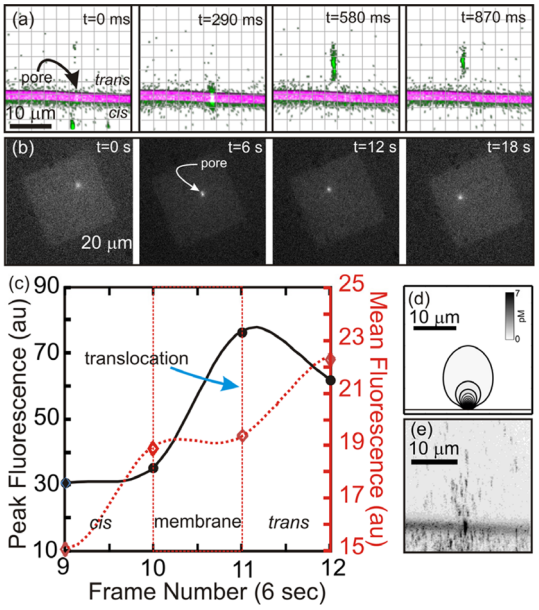

Figure 2. Linear 20 kbp dsDNA intercalated with YOYO-1 translocating through a 3.8 nm diameter pore in a 30 nm thick silicon nitride membrane. (a) Confocal ($x-z$) cuts through the membrane showing the translocation of DNA-YOYO-1. The bright, ellipsoidal feature is associated with a single molecule of DNA. (b) Fluorescent micrographs showing dsDNA-YOYO-1 translocating from the *cis*-side of the partially transparent membrane, exiting on the *trans*-side. (c) Integrated intensity showing the peak (black) intensity and mean (red) intensity in the field shown above per frame. The peak fluorescence indicates the frame in which a translocation occurs, while the mean fluorescence indicates the position of the membrane. (d) Finite-element simulation of DNA translocation through a nanopore with the same geometry as in (a–c) and a surface charge density of $\sigma = -7$ mC/m^2. Contours of the concentration of DNA as it translocates through the pore are calculated in steady-state. At a distance of 10 μm above the membrane, the distribution of DNA molecules has a fwhm of 8.8 μm. (e) Maximum projection of 2600 frames as in (a), showing the distribution of DNA above the membrane in agreement with (d).

which is slower than prior estimates obtained for a similar pore.[39] Using YOYO-DNA with a transmembrane bias <1 V, no signature of a translocation was observed in either the current or fluorescence in the 30 nm thick membrane; however, using a nominally 10 nm thick membrane with a same sized pore, current blockades were observed for transmembrane biases as low as 150 mV. For thinner membranes, the number of surface charges in the pore is likely to be smaller, which leads to a reduction in the voltage required to induce a translocation (see below).

Figure 2a shows a series of confocal fluorescence micrographs that captures the translocation of a single molecule across a 30 nm thick solid-state membrane through a 3.8 nm diameter pore with a 1 V transmembrane voltage applied. This sequence of images was obtained from an $x-z$ scan (along the pore axis) through the membrane when a dilute, 4.5 pM, solution of monodispersed 20 kbp dsDNA-YOYO in 100 mM KCl was flowed into the *cis*-chamber of the microfluidic device. The $x-z$ scan was implemented using a resonant 8 kHz laser scanner along x and a galvanometer stage that scans the z (optic) axis to produce the unreconstructed confocal image shown in (a). In this analysis, an image was acquired every ~290 ms with an acquisition time of 25 ms. At t = 0 ms, a fluorescent molecule approaches the pore from a distance of ~3 μm away from the pore. In the next frame (t = 290 ms), the molecule is depicted as translocating across the membrane through the pore. At t = 580 ms, the molecule is found on the *trans*-side of the membrane 10 μm above the *trans*-orifice. Finally, at t = 870 ms, the molecule remains about 10 μm above the *trans*-orifice although it is displaced about 1 μm laterally from the position at 580 ms. The low excitation intensity (500 nW) allowed for a photochemical lifetime of several minutes. After accounting for the confocal acquisition parameters, we found that a single trapped dsDNA loses only about 50% of its fluorescent intensity within 10 min. The fluorescence image associated with the single YOYO-DNA molecule shown in each frame appears as an elongated ellipse.

The fluorescent images attributed to single molecules in solution on the *cis/trans*-side of the membrane were estimated to extend laterally about Δx = 650 ± 40 nm (averaged over 100 molecules) with the largest lateral extent being Δx_{max} = 1.6 μm, which was greater than the lateral confocal resolution, estimated to be $\sigma_{xy} = 0.51\bar{\lambda}/NA$ = 212 nm, where $\bar{\lambda} = \sqrt{2}\lambda_{ex}\lambda_{em}/(\lambda_{ex}^2 + \lambda_{em}^2)^{1/2}$ = 499 nm with λ_{ex} = 488 nm and λ_{em} = 510 nm. The lateral resolution, measured using monodispersed 20 nm fluorescent nanospheres (FluoSpheres Carboxylate-Modified Microspheres, Invitrogen), was σ_{xy} = 499 ± 25 nm. On the other hand, the axial resolution with a pinhole fixed at 1 Airy unit (AU) was estimated to be much larger: $\sigma_z = 0.88\bar{\lambda}/(n-(n^2 - NA^2)^{1/2})$ = 580 nm, where n is the index of the immersion liquid (electrolyte). The measured axial resolution was σ_z = 1.740 ± 0.140 μm. With the pinhole set to 1 AU, the optical slice thickness and the axial resolution were not the same. The full width at half-maximum (fwhm) of the intensity distribution was determined by the emission side diffraction pattern and the geometric optical effect of a pinhole set to PH = 1 AU = (1.22$\bar{\lambda}$/NA) = 705 nm; that is

$$\Delta z = \sqrt{\left(0.88\frac{\bar{\lambda}}{n - \sqrt{n^2 - NA^2}}\right)^2 + (\sqrt{2}n\mathrm{PH}/\mathrm{NA})^2}$$

which was comparable to the measured value. However, neither of these estimates actually determined the z axis resolution since, under the conditions of the experiment, mechanical fluctuations in the thin #0 coverslip (80–130 μm thick) supporting the microfluidic compromised the performance. Thus, at minimum Δz = 2.5 ± 0.6 μm, and so, on average, a single DNA molecule appears to be about Δz = 3.0 μm along the z

axis and oriented perpendicular to the membrane without exception. While the area (30 μm × 30 μm) scanned for fluorescence detects every molecule in z and x, the depth of focus is only ±1 μm(~2 × σ_{xy}) along y so that, assuming a Gaussian point spread function, ~10% of the fluorescent intensity will still be detected. Therefore, images like that shown in Figure 2a are not always able to capture the entire trajectory of the ejected molecules.

Under these conditions, it has been established that dsDNA behaves almost like an ideal polymer chain, primarily because it comprises a double helix of two polymer chains.[35−38] Therefore, the fluorescence can be accurately described by a worm-like chain (WLC) behavior. The effective diameter of DNA was estimated to be much greater than the 2 nm diameter helical structure, or the solvated structure, which is about 2.6−2.9 nm in diameter, or the Debye screening length, which is approximately 1 nm in 100 mM KCl.[40] If DNA is modeled as a WLC, then the mean-square end-to-end distance for a linear chain is given by $(\langle L^2\rangle)^{1/2} = b\sqrt{N} \equiv \ell$, where b is the Kuhn segment (which is twice the persistence length) and N is the number of segments.[35] The measured persistence length, associated with YOYO-intercalated DNA, is supposed to be 35 nm (standard deviation of 18.6 nm) with standard error of the mean 2.8 nm so that $N \sim 97$,[35] which is consistent with other estimates of native DNA.[41] The radius of gyration, R_g, is given by: $(\langle R_g^2\rangle)^{1/2} = (\ell/6) = b(N/6)^{1/2} \equiv R$. On the other hand, the hydrodynamic radius R_h of an ideal linear chain, defined as the radius of a hydrodynamically equivalent sphere, is supposed to be smaller than R_g (*i.e.*, $R_g \approx 1.24R_h$). For this DNA, it was estimated that $l = 609$ nm, $R = 115$ nm, and $R_h \approx 93$ nm, assuming $b = 70$ nm and $N = 97$, which is consistent with the lateral extent of the image (650 ± 40 nm). The membrane appeared as a horizontal band of scattered laser light spanning each frame—it does not fluoresce. The weak light scattering from the thin nitride membrane, combined with the limited resolution, makes the 30 nm thick membrane appear thicker than it actually was.

Complementary to Figure 2a, Figure 2b (which bears no relation in time to the data shown in Figure 2a) shows a series of images that follows a single molecule as it migrates toward and eventually translocates across the membrane through a 3.8 nm diameter pore. This wide-field fluorescent image sequence had a higher depth of focus allowing for tracking the molecule for a longer period of time. Since the optical focus was set in the plane of the membrane, when the molecule translocates through the pore, it came to a sharp focus and, correspondingly, the peak fluorescence was maximized, as illustrated in Figure 2c. Thus, the location of the pore could be identified unambiguously, despite the limited resolution. The increase in the overall fluorescent intensity with time shown in Figure 2c, which was associated with the molecule moving across the weakly scattering membrane toward the microscope objective, served to pinpoint the translocation event in time, as well.

The molecule appeared to move in the x−y plane above and below the pore a distance ~4.4 ± 1.3 μm between frames in Figure 2b, which is consistent with diffusion over a length $L = (Dt)^{1/2} = (1.572\ \mu m^2/s \times 6\ s)^{1/2} = 3.1\ \mu$m. The motion along the z axis between frames shown in Figure 2a is inconsistent with diffusion; however, since the molecule appears to travel $\sigma_z \sim 5.7 \pm 0.7\ \mu m > L_d = 675$ nm. This large range of z motion is attributed to the combined action of the electrophoretic force and the electro-osmotic flow on the molecule.

Simulations of the motion performed using a FE model (COMSOL v4.2; see Methods) under similar conditions reveal that the velocity of the molecule in the pore can be very high (~60 cm/s along z), assuming that the viscosity of water in the pore is approximately $\eta_{pore} = 10$ mPa·s (10× that of bulk water $\eta_{pore} = 1.002$ mPa·s),[42,43] which is consistent with the duration of the blockade current. However, the velocity of the molecule collapses immediately (15 nm) above the membrane to a value <5 mm/s, forcing the ejected DNA into a plume 13 μm long with a 6.8 μm (fwhm) width above the pore, as illustrated in Figure 2d. The DNA velocity is slowed by the electro-osmotic flow associated with the double layer of counterions of the charged pore walls, which forces water in the opposite direction (for a negatively charged pore) through the pore and diminishes the electrophoretic effect.[34] Correspondingly, the superposition of 2600 consecutive measurement frames covering 754 s of data (including the data of Figure 2a) shown in Figure 2e indicates that the distribution of the 38 DNA molecules exiting the pore seems to be confined in a plume, as well.

Taken altogether, the images along with the simulations support the interpretation that the bright fluorescence observed at $t = 290$ ms, showing a molecule that appeared to span the thickness of the membrane, likely corresponds to dsDNA localized near the pore for an interval greater than the average translocation time ($t_D \sim 600\ \mu s$), but ≤25 ms, which was the duration of the acquisition window. The rate at which such events occurred was about 0.05 molecules/s (38 molecules translocating in 754 s) for this pore. This rate coincides with the mean DNA flux of 0.045 molecules/s (7.7 nmol nm^{-2} s^{-1}) derived from FE of a 3.5 nm diameter pore, which takes into account the concentration of the DNA (on the *cis*-side of the membrane), the diffusion, the electrophoretic migration into the pore due to the electric field, and the electro-osmotic flow and corroborates our estimate of the electric field distribution. The trajectory of the molecule along z both prior to and after it exits the pore was profoundly affected by electrophoretic forces and the

electro-osmotic flow, while diffusion seemed to play a more substantive role in determining the *x* and *y* components.

Visualization of Linear DNA Translocations and Correlation with the Pore Current. Simultaneous current measurements and image acquisition to capture the dynamics of the translocation process remains a challenge because a single line scan can repeat only once every 125 μs (=1/(8 kHz)) at best and because the electrical photocurrent generated by the focused laser excitation on the membrane can obscure and even saturate the pore current for the duration of the exposure, depending on the bandwidth and gain of the current amplifier. Furthermore, it is difficult to effectively shield the sample from electric interference associated with the microscope, hence the measured rms current noise (25 pA) is higher than when measured without having the microscope (10 pA). Nevertheless, fluorescence images acquired under these conditions, like that shown in Figure 3a, can still indicate the translocation of a single molecule and can localize its position to within 3 μm of the *cis*- and *trans*-orifices routinely. Current measurements performed at the same time that these images were acquired revealed current transients associated with a single-molecule translocation. These transients exhibited a multifaceted structure. For example, the inset shows that there was a blockade $\Delta I/I_0 = 0.42 \pm 0.11$ below the open pore value (I_0 = 3.5 $\pm$ 0.5 nA) with a duration lasting t_D < 120 μs; followed by a much shallower blockade within the noise of the open pore current, with a duration ~800 μs; followed by a sharp enhancement of the current over the open pore value $\Delta I/I_0 = 0.65 \pm 0.11$ of nearly 1 ms in duration; followed by an enhancement $\Delta I/I_0 = 0.14 \pm 0.05$ that persists for >50 ms. Following Aksimentiev *et al.*,[13] we expect that the presence of DNA in the pore reduces the ionic current through it. However, when DNA rapidly exits the pore, clouds of Cl^- and K^+ ions that were accumulating near the pore's orifices are released, resulting in a transient increase of the total current above the open pore level. Due to the wide field of view, it is unlikely that another fluorescent DNA could interfere with this current measurement. Thus, we interpret these data to show that DNA blockades the pore for only a limited duration (<150 μs) with the subsequent convection of counterions accounting for the enhancement above the open pore value, as predicted.[13]

In contrast, Figure 3b shows an extraordinary event in which a linear plasmid is trapped in the same nanopore for a duration exceeding 2.32 s so that the progress of the molecule through the pore can be easily tracked. We assume that the current blockade in the pore, which was initiated ~8.4 s prior to the time course shown in the figure, is due to a nonfluorescent species. As evident from the fluorescence, a single dsDNA is captured by the pore near 1.45 s and

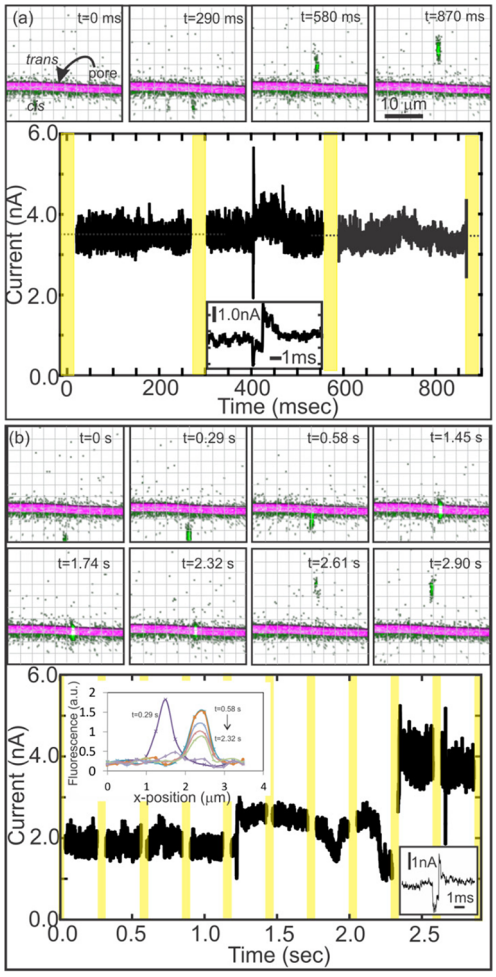

Figure 3. Direct visualization of single linear 20 kbp DNA plasmids translocating through a nanopore along with concurrent measurements of the current. (a) Confocal *x*−*z* cuts of fluorescence DNA translocating through the same 3.8 nm diameter pore shown in Figure 2, along with the corresponding current measurements. The fluorescence is acquired in a 40 ms window every 290 ms; the yellow-shaded regions superimposed on the current time-course indicate when the confocal fluorescence measurements are performed. The fluorescence shows an ellipsoidal feature approaching the membrane at *t* = 290 ms and exiting the pore at *t* = 580 ms. The corresponding current measurement shows a current transient near *t* = 400 ms that includes a very short duration blockade (120 μs) as well as an enhancement above the open pore value (I_0 = 3.5 nA) that extends for nearly 50 ms following the blockade. (b) (Top) As above, confocal *x*−*z* cuts of fluorescence DNA translocating through the same 3.8 nm diameter pore, (bottom) along with the corresponding current measurements performed with a nonfluorescent species blockading the pore. The fluorescence shows a single molecule of dsDNA approaching the membrane at *t* = 0.29 and 0.58 s. The corresponding current measurement shows a current transient near *t* = 1.45 s which is interpreted as the molecule entering the *cis*-orifice. The molecule translocates slowly through the already blockaded pore only exiting between *t* = 2.32 and 2.61 s. In this case, the current through the pore is modulated by the translocating DNA. The lower inset shows a magnified view of a current transient through the unadulterated pore, which occurs near 2.6 s. The top inset shows a plot of the positional dependence of the fluorescent intensity from *t* = 0.29−2.61 s illustrating that changes in the fluorescent volume coincide with the observed change in the current.

proceeds to modulate the current as it presumably reconfigures to thread the end of the strand into the pore and finally translocate across the membrane at 2.32 s, which coincides with the deepest current blockade. A detailed comparison of the blockade current (see inset for Figure 3b) with the fluorescent images reveals that the fluorescence diminishes to a minimum at t = 2.32 s; that is, the integrated (fluorescent) intensity is approximately 50% less than the value found at t = 1.45 s or t = 1.74 s. We assume that the changing intensity corresponds to a reconfiguration of the DNA with the minimum intensity associated with the maximum occlusion of the pore by the molecule and deepest blockade. In addition, the distribution of the fluorescence over the x position changed from 2.03 to 2.32 s: the center of the intensity shifts to the right by 40 $\pm$ 20 nm, which is interpreted as a change in the DNA conformation at the pore immediately before it exits at 2.32 s. At t = 2.61 s, the dsDNA drifts to a position about 10 μm above the *trans*-orifice and the current returns to the open pore value of I_0 = 3.5 $\pm$ 0.5 nA, indicating that both the DNA and the nonfluorescent species have exited the pore. Evidently, the pore returns to an unadulterated (pristine) condition since another single DNA molecule is observed translocating across the membrane in the interval between 2.61 and 2.90 s as indicated by the measurement of a blockade ($\Delta I/I_0$ = 0.43 $\pm$ 0.11, t_D = 600 μs) at t = 2.62 s (which is magnified in the inset) followed by an apparent enhancement of the current above the open pore value. Thus, the DNA seems to occlude the nanopore producing a current transient that corresponds to a blockade when the fluorescent volume is minimized.

The coincidence of a nonfluorescence species with fluorescent DNA in the pore and the concomitant slowing of the translocation shown in Figure 3b implies that, if the DNA concentration is too high and multiple molecules are incident on the *cis*-orifice, a nanopore could become susceptible to clogging, which could adversely affect the current regardless of whether or not a blockade is observed. As illustrated in Figure 4a, this happened even at a relatively dilute concentration of DNA of 5 pM. Figure 4a,b juxtaposes the results of intermittent fluorescence measurements obtained concurrently with measurements of the pore current through a 5.8 $\pm$ 0.2 nm diameter pore in a nominally 30 nm thick membrane. For these measurements, both the *trans*- and *cis*-side of the membrane were immersed in 10 mM TE buffer and 10 mM KH_2PO_4/NaOH, but YOYO-1 intercalated linear 20 kbp dsDNA at a concentration of 4.5 pM was introduced on the *cis*-side only—which translates to 1 molecule/(22 μm)^3. During the measurements, the transmembrane voltage was pulsed at 1, 0.5, 0.25, 0.125, and 0.150 V for 20, 15, 18, 60, and 20 s, respectively, as represented in the lower portion of Figure 4b. Confocal images were acquired every 1 s and the acquisition time for each x–z scan at

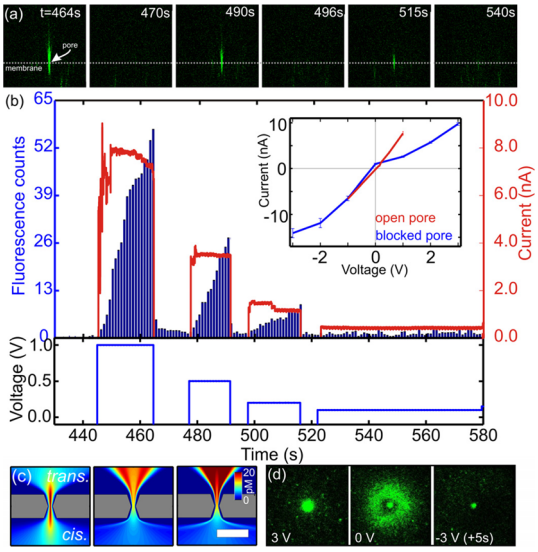

Figure 4. DNA accretion in a nanopore: 20kb dsDNA-YOYO-1 at a concentration of 4.5 pM reversibly accumulates near a 5.8 nm pore in a 30 nm thick silicon nitride membrane pore at pH 5 when a large enough attractive potential is applied. (a) Confocal x–z scans of the fluorescence as a function of voltage corresponding to snapshots taken from (b). At t = 464 s, the voltage is 1 V, while at t = 470 s, the voltage is 0 V, *etc.* The t = 464 s image illustrates an accumulation of fluorescent dsDNA at the pore. (b) (Top) Integrated fluorescence intensity (blue bars) obtained from a 10 μm square-shaped ROI centered at the pore, along with the current (red line) through the nanopore. For V > 0.25 V, the current diminishes with time coincident with the accumulation of DNA. (Bottom) Corresponding transmembrane bias voltage. Inset: Change in the current–voltage characteristic with DNA accumulation relative to the open pore obtained in the absence of DNA. The I–V characteristic is asymmetric, and the pore current is diminished—the larger the voltage, the more the current is suppressed—when DNA accumulates at the orifice. (c) Contour plot showing the simulated steady-state DNA concentration in cross section of a 5.8 nm pore in a 30 nm thick membrane with a zeta-potential of ζ = −20 mV. The applied potential is either +3 V (left), +1 V (center), or 850 mV (right). The bulk DNA concentration in the *cis*-side (below the membrane) is 5 pM. The scale bar indicates 30 nm. (d) Fluorescent images obtained in steady-state as a function of the transmembrane voltage 5 s after it is switched, illustrating accretion of 20 kbp dsDNA at a concentration of 4.5 pM around the same pore as in (a) immersed in an electrolyte consisting of 10 mM KH_2PO_4, NaOH at pH 5. As the voltage increases from −3 to +3 V, the attraction of DNA to the pore turns to repulsion, and the fluorescent DNA is dispersed as evident from the increase in the fluorescent volume at 0 V. Even when +3 V is applied for >10 s, the fluorescence in the neighborhood of the pore persists, indicating that the DNA adheres to the pore.

128 ms (256 lines × 4 line accumulations × 125 μs line scans).

The confocal x–z scans shown in Figure 4a are typical snapshots illustrating accumulation of dsDNA at the pore observed at 464, 470, 490, 496, 515, and 540 s, which corresponds to transmembrane biases of 1, 0.0, 0.5, 0.0, 0.25, and 0.0 V, respectively. It is evident from the increase in fluorescent intensity that DNA is accumulating near the pore. During a voltage pulse, the fluorescence increases with time, indicating an accretion of DNA in the region of interest (ROI), but

the change in current is more gradual and less precipitous. Analyzing the slope of the fluorescence as function of voltage (1 V:3.0 au/s; 0.5 V:2.0 au/s; 0.25 V:0.3 au/s), we observe a 10-fold depreciation in the capture rate when switching from 1 V down to 250 mV. Moreover, the fluorescence returns to the noise floor between pulses when the voltage relaxes to zero. As indicated in the inset to Figure 4b, the accretion of the DNA to the pore affects the current−voltage characteristics, which shows that, in the absence of DNA, the pore current scales nearly linearly with the transmembrane voltage over the range of −1 to 1 V (red line), but during voltage pulses with dsDNA on the *cis*-side of the membrane, DNA accumulates near the pore and the fluorescence increases while the current decreases (blue). The current is a linear (within 5%) function of voltage in the absence of DNA, implying a nearly symmetric distribution of surface charge in the symmetric biconical model for the pore (inset to Figure 4b), whereas when DNA is injected at the negative electrode, it introduces an asymmetry in the current−voltage characteristic, presumably due to an imbalance in the charge near the pore associated with DNA near the *cis*-orifice.[22]

These data support the contention that the dsDNA in the neighborhood of the *cis*-orifice obstructs the pore current at this concentration for voltages in the range between 0.2 and 1 V. This assertion is corroborated by the FE analysis represented in Figure 4c. The figure shows that at a +1 and +0.85 V bias (middle and right) the DNA below the *cis*-orifice of a nanopore with a zeta-potential (the electrostatic potential of the charged surface in an electrolyte at the double layer[44]) of $\zeta = -20$ mV is confined to a narrow plume about 12 nm wide, which is consistent with the resolution limited width shown in Figure 4a. Since the simulations treat the DNA as a point particle, we assert that the finite size of 20 kbp DNA leads to crowding and a blocked pore. As indicated by eq 3 in the Supporting Information, the surface charge density corresponding to $\zeta = -20$ mV and 10 mM electrolyte is $\sigma = -4.7$ mC/m^2, which translates to ∼33 charges inside a 5.8 nm biconical pore in a 30 nm membrane. The accumulation of dsDNA below the nanopore increases as the applied voltage approaches a translocation threshold, which depends on the surface charge density of the pore. The simulations reveal that the translocation threshold in a 30 nm thick membrane is about 1 V (Figure 4c (center)). While dsDNA may translocate through the pore, there still appears to be an accumulation of dsDNA at the orifice on the *cis*-side. Below this threshold, shown in Figure 4c (right), the dsDNA does not accumulate at the orifice appreciably above the background concentration. Thus, the accumulation of dsDNA occurs when the applied voltage is near the translocation threshold voltage of the pore of a given surface charge density. For the same surface charge density, a thinner 10 nm thick membrane contains only ∼7.5 charges in the pore and the threshold voltage is similarly reduced to only 650 mV.

The accumulation of dsDNA in the experiments represented in Figure 4a,b seems to be reversible in both simulation and experiment; that is, the dsDNA diffused away from the pore when the transmembrane voltage vanished. There were conditions for which the dsDNA adhered to the membrane near the pore whether or not a voltage was applied, however. Figure 4d shows fluorescent images obtained in steady-state (left and right) as a function of the transmembrane voltage 5 s after it was switched, illustrating (again) the accretion of linear dsDNA at a concentration of 4.5 pM around a 5.8 nm diameter pore in a 30 nm thick membrane immersed in an electrolyte consisting of 10 mM KH_2PO_4, NaOH at pH 5. As the voltage decreased from 3 to −3 V, the attraction of DNA to the pore diminished and the fluorescent dsDNA was dispersed as evident from the increase in the fluorescent volume at 0 V. Eventually, at a repulsive bias of −3 V, the fluorescent volume reached a minimum—confined to the immediate vicinity of the pore, but even when this voltage was applied for >10 s, the fluorescence in the neighborhood of the pore persists, indicating that the dsDNA adhered to the pore—similar observations have been made on ∼100 nm diameter pores and attributed to the effect of surface charge in the pore.[23]

FE indicates stark differences between small and large diameter pores. While, for the same transmembrane potential, the electric field is greater than 2-fold higher inside and near a pore with a 3.5 nm than it is for a 20 or 100 nm diameter pore (see Figure S2 in the Supporting Information), the electric field extends much farther beyond the membrane into the surrounding electrolyte as the pore diameter increases. For example, at a distance of 1 μm above the pore, the electric field is ∼24-fold higher for a 100 nm diameter pore than for a 3.5 nm diameter pore. On the other hand, for a 3.5 nm diameter pore, the electric field is confined to a region just above the pore, making it less likely to capture a molecule (or visualize it). Likewise, a 10 nm thick membrane shows a higher field than 30 nm thick membranes, but the disparity is not nearly as prominent as with the diameter. The effects of changes in the concentration and zeta-potential are also negligible in comparison to the effect of pore diameter and membrane thickness. To illuminate the differences, we have measured the current and fluorescence of a circular plasmid DNA translocating through a pore with a diameter comparable to the bending radius.

Visualization of Circular DNA Translocations and Correlation with the Pore Current. While many eukaryotic genomes are linear, prokaryotic genomes and most cloned DNA constructs are circular. Thus, analyzing circular DNA

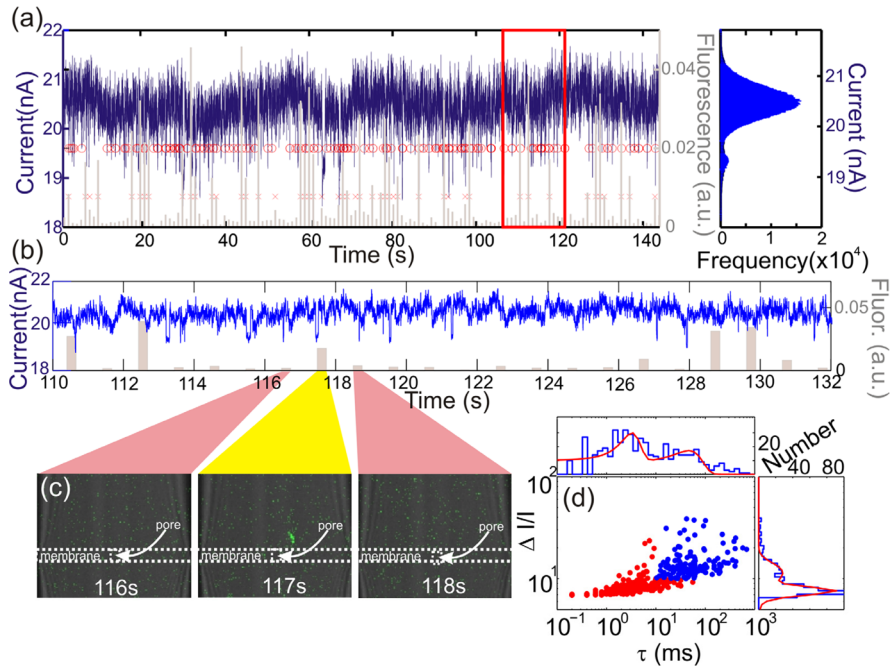

Figure 5. Simultaneous measurements of the pore current and fluorescence associated with circular dsDNA plasmids interacting with a ~24 × 17 nm^2 cross section pore in a silicon nitride membrane. (a) Electrolytic current through the nanopore (blue) and fluorescence recorded in 1 s intervals, denoted by the gray bars. A red ○ indicates a current event meeting the criteria for a plasmid translocation, and a red × indicates an image showing a plasmid on the *trans*-side. Inset: histogram showing the open pore current near 20.5 nA and the blockade current near 19.5 nA. (b) Expanded view of (a) showing the current and fluorescence in the time frame between 110 and 132 s. (c) Series of three *x*−*z* slices showing an overlay of transmission and fluorescence, illustrating a translocation in frame 117 and an open pore in frames 116 and 118. The corresponding current blockade was observed in frame 117 and indicated in (b), while no fluorescence was in frames 116 and 118, even though there are current blockades, suggesting bounces. (d) Scatter plot of the 475 current events detected in (a). Projections of both axes are plotted as histograms on each side. Two Gaussians were fit to distributions of the translocation durations (τ) and the blockade depths ($\Delta I/I_0$). The events colored blue are in regions that match the criteria for plasmid translocations.

using a nanopore is also of interest, especially for accurate control of single-cell transfection.[30] Provided that each molecule can be counted with high enough fidelity using a current measurement, transfection *via* electroporation using a nanopore offers single-molecule accuracy.

For a DNA molecule to become circular, it has to be long enough to bend into a circle with the correct number of bases so that the ends are properly rotated to allow them to bond. The B form of the DNA helix twists 360° per 10.4−10.5 bp in the absence of torsional strain. Thus, with an integral number of turns of the DNA helix (*i.e.*, multiples of 10.4 base pairs), the minimum length for a circular DNA plasmid is around 416 base pairs (or about 141 nm). We formed a circular plasmid 8624 bp long, which likely exists in a supercoiled conformation corresponding to over- or under-winding of the strand. This conformation is too stiff to translocate through a 1−10 nm diameter pore. However, the circular plasmid can be forced to denature in the pH 9 electrolyte due to the disruption of the hydrogen bonding. For an ideal circular chain like this in the WLC model, $L = 0$ by definition and the radius of gyration is $(\langle R_g^2 \rangle)^{1/2}/2 = b(N/12)^{1/2} \equiv R_c$, which is shorter than that of a linear chain with the same contour length. (Thus, due to the relatively tight conformation compared to linear DNA, supercoiled DNA could actually migrate faster through a pore than linear DNA.)

Figure 5a juxtaposes measurements of the fluorescence in a ROI (30 × 20 × 2) μm at the *trans*-orifice of a 23.8 × 16.6 ± 0.2 nm pore in a membrane that is nominally 30 nm thick with an electrolytic current associated with a 8.6 kbp circular plasmid translocating through it at a 1 V bias. The figure illustrates that the electrolytic current through the open pore was approximately 20.5 ± 0.5 nA, but frequently (about once every 2−3 s), current blockades were observed occurring in the range between 19 and 20 nA. The result of repeated fluorescence measurements (every 1 s with a 250 ms acquisition window) revealed single plasmids in or around the pore as represented by the gray bar graph superimposed on the current trace. We observed 367 molecules in 142 s (2.6 molecules/s) for a concentration of 5 pM on the *cis*-side of the membrane. Figure 5b offers a magnified view of the same data in the time frame between 110 and 132 s. In particular, the confocal *x*−*z* scan offered in Figure 5c taken at 117 s, which corresponds to the Δt = 85 ms long, $\Delta I/I = 0.053$ current blockade observed at 117.7 s, shows fluorescence on the *trans*-side of the membrane.

When a fluorescent molecule was found on the *trans*-side of the membrane, a translocation event was tallied. Fluorescent events and current blockades are indicated by the red crosses and circles, respectively, in Figure 5a. Conditioned on the observation of fluorescence, the coincidence between fluorescence and current blockades observed in the range of 19−20 nA was very high—out of 49 fluorescent events tallied, a current blockade was observed every time. However, fluorescent events were not tallied every time a current blockade was observed. For example, current blockades $\delta t \sim 10$ ms long with $\Delta I/I = 0.05 \pm 0.01$ were observed near 116 and 118 s, as shown in Figure 5b, but no fluorescence was detected on the *trans*-side of the membrane in the corresponding snapshots acquired near the same time shown in Figures 4c. These short duration current blockades with associated fluorescence on the *cis*-side of the membrane were conjectured to be associated with DNA molecules "bouncing" off the pore in a configuration that does not admit to translocation; the molecules cannot be straddling the pore since no fluorescence was observed there.[5,19−21] Finally, other short time, shallow current blockades are observed that are not correlated to fluorescence at all (on either the *cis*- or *trans*-side). These cannot be attributed to smaller fragments of DNA since they would still fluoresce, albeit weakly. Instead, these events must be due to a species without perceptible fluorescence, possibly not even DNA.

Using a custom script written in MATLAB, all current events were characterized based on their dwell time and percentage blockade current in the interval showed in Figure 5a; the corresponding scatter plot is shown in Figure 5c. The criterion used to tally a translocation is $\delta t > 10$ ms and $\Delta I/I > 0.039$. Out of 367 current blockades matching the criteria for a translocation, only 49 fluorescent events were observed. This discrepancy between the number of blockades and fluorescent events was accounted for by the fact that the fluorescence was measured only 25% of the time; that is, the inter-arrival time is sometimes shorter than 250 ms, so that multiple blockades occur when only one fluorescent event was tallied; some fluorescent molecules were out of the confocal volume, which is small $30 \times 30 \times 2$ μm in order to keep the frame rate high. Therefore, only a slab of the 6 μm diameter plume as shown in Figures 2d,e is monitored, and so only ~50% of the translocation events are detected.

CONCLUSION

In conclusion, visualizing the motion of fluorescent DNA while performing pore current measurements using the most dilute concentrations reported so far reveals single molecules translocating across a thin silicon nitride membrane through nanopores comparable in size to a hydrated double helix in a linear plasmid or the bending radius of a circular plasmid. The motion of the molecule near the pore is affected by both electrophoresis and the electroosmotic flow. In a large 24×17 nm pore, there is a close correspondence between blockades in the pore current and translocations observed in the fluorescence. On the other hand, blockades in the pore current only rarely coincide with observations of a translocation in the fluorescence in a 3.8 nm diameter pore. The large electric field within and near the small diameter pore may account for this discrepancy: the molecular motion in and around the 3.8 nm pore is just too fast to be captured with the type of confocal microscopy used here.

FE reveals that the electric field is tightly focused in a 3.5 nm diameter pore relative to larger diameter pores. While the electric field is 2× larger for the same voltage, it extends only a few nanometers above the membrane for a 3.5 nm diameter pore. In contrast, the electric field at a distance of 1 μm above the pore is ~24-fold higher for a 100 nm diameter pore than for a 3.5 nm diameter pore. The corresponding potential energy indicates that the capture volume, defined by a potential of k_BT, for a 20 nm diameter pore is a prolate hemiellipsoid with a semimajor (radial) and semiminor axes of 84 and 72 nm, respectively (see Supporting Information Figures S3 and S4). On the other hand, for a 3.5 nm diameter pore, the capture volume has a 33 nm semimajor axis and a 20 nm semiminor axis. In terms of the total volume, the 20 nm pore's capture volume is ~32-fold larger than that of the 3.5 nm pore, which correlates with the disparity measured in the event rate for 24×17 nm the pore (2.6 Hz) compared with the 3.8 nm pore (0.05 Hz). These translocation rates are in close correspondence with simulations of the average DNA flux (0.045 Hz), which support our estimate for the electric field distribution. Moreover, these results have implications for the response time.

The rate of capture, which is inversely proportional to the response time, is related to the product of the analyte concentration and capture radius;[45] so a reduction in the capture volume either increases the response time or increases the minimum detectable concentration. Thus, the detection efficiency is manifestly affected by the pore diameter. On the other hand, the high electric field and narrow field distribution above the pore are ideally suited for electroporation since only a minimal area of the cell membrane would be affected.[30] Thus, the model for the pore, the electric field, and the DNA concentration used in the simulations are consistent with the observed frequency of translocations.

For electrolyte concentrations, pH and electric fields used prevalently: an accumulation of linear DNA obstructing the orifice of a 5 nm diameter pore affects the pore current even in the absence of a translocation; linear DNA sticks to the synthetic pore in concentrated electrolyte even in the absence of an applied field; the

pore clogs with DNA irreversibly at pH 5. While at pH 8, the small 3.4 nm diameter pore clogs, especially at high field, but the clogging is reversible. In contrast, at the same pH, the larger 24 × 17 nm pore diameter does not clog at all. We attribute the clogging to DNA sticking to the effect of surface charges in the pore, which may be modified by varying the pH or by using a thinner membrane.

METHODS

Biomolecules. To visualize a translocation, we used monodispersed, linear double-stranded DNA (dsDNA) and circularized plasmid DNA intercalated with YOYO-1 iodide dye (Invitrogen). YOYO-1 has a 491/509 nm peak fluorescence excitation/emission, a molar extinction of 98 000 M^{-1} cm^{-1}, and a quantum yield of 0.52. These values were determined for DNA complexes in 10 mM Tris, 1 mM EDTA, 50 mM NaCl, pH 7.4.[35−38] A 20 or 8.6 kbp circular plasmid dsDNA was added to a YOYO-1 dye solution (40 mM Tris-acetate, 2 mM EDTA, pH 8.0) for a final ratio of 5:1 nucleotides to dye molecules. This mixture was then incubated for 90 min at room temperature then stored at 4 °C. A 25 pM concentration of DNA-YOYO was added to 100 mM KCl (pH 8.0).

Nanopores. A nanopore is created by sputtering through silicon nitride membranes <30 nm thick on a silicon handle wafer, using a high-energy (300 kV), tightly focused electron beam emanating from a field emission source in a FEI Titan 80-300 transmission electron microscope (TEM) operating in nanoprobe mode as described elsewhere.[30] From TEM images taken at different tilt angles, it was inferred that the pore geometry is biconical each with <20° cone angle. Subsequently, the chip containing the membrane is plasma bonded to a multilevel microfluidic device. The plasma bond seals the chip into the microfluidic between the two *vias*, leaving the pore as the only connection between the *cis*- and *trans*-channels, as illustrated in Figure 1. The *cis*-reservoir has a volume of ∼100 μL, while the *trans*-reservoir *via* has a volume of ∼6 nL.

To characterize the pore, a transmembrane voltage was applied and current was measured at 23 ± 1 °C with a MultiClamp 700B amplifier and digitized with a DigiData 1440A (Molecular Devices) using Ag/AgCl electrodes embedded in each fluidic channel at a sampling rate of 100 kHz. For potentials >1 V, the potential was applied and the current measured with a picoammeter/voltage source 6487 (Keithley) with a signal rise time of 1 ms.

Microfluidic. A silicon chip supporting a silicon nitride membrane with a pore in it was embedded in a microfluidic device formed from poly(dimethylsiloxane) (PDMS) consisting of two microchannels configured to independently address the *cis*- and *trans*-sides of the membrane through *vias* using methods reported elsewhere.[30] The entry channels were all 250 μm wide and 75 μm high, with *vias* (see Figure 1d) that are 600 × 325 and 50 μm thick. The silicon chip was tightly sealed to the PDMS *trans*-microfluidic channel with a plasma bonding process (Harrick PDS-001) that exposed the chip and PDMS to an oxygen plasma at a power of 30 W for 180 s. At the same time, to provide optical access, we likewise sealed the *trans*-channel in the PDMS to a #0 cover glass (Corning) using the same bonding strategy described above. We subsequently tested the seal against a 30 nm thick silicon nitride membrane without a pore in 100 mM KCl pH 8 for >6 months without failure; the leakage current was <8 pA at 1 V. Finally, the microfluidic is clamped on a high-speed (8 kHz) scanner stage on the confocal fluorescence microscope.

Confocal Fluorescence Microscopy. Fluorescence data were collected using a Leica TCS SP5 II (Leica Microsystems) confocal microscope with enhanced, hybrid GaAsP detectors for improved sensitivity to fluorescence. All confocal images were acquired using an HCX PL APO lambda blue 63× 1.2 NA (Leica) water immersion objective using a 488 nm argon excitation laser at a power of 500 nW.

Finite-Element Simulations. The electrophoretic and electro-osmotic flow of ions through the nanopore was simulated using a FE model (COMSOL v4.2). The potential across the nanopore was determined by solving the Poisson equation:

$$\nabla^2 V = -\rho/\varepsilon\varepsilon_0 \quad (1)$$

where V is the potential, ε is the relative dielectric permittivity of water, and ε_0 is the vacuum permittivity. In the electrolyte, ε = 78.5 and the volume charge density is given by $\rho = \sum z_i n_i$, where z and n are the valences and number density of each ion of species i, respectively. In the silicon nitride, ε = 9.7 and ρ = 0. The surface charge density in the pore was a boundary condition. The electro-osmotic flow in the nanopore was determined by solving the Stokes equations:

$$\nabla \cdot v = 0 \text{ and } \nabla p = \eta \nabla^2 v \quad (2)$$

where v is the velocity, p is the pressure, and η is the viscosity of water. The viscosity of water, η, was assumed to be larger in the confined geometry of the nanopore; thus η was varied with respect to distance from the pore as $\eta(z) = (\eta_{pore} - \eta_0)\exp[-(4.7/L)^2] + \eta_0$, where z is the axial position of a pore centered at z = 0; L = 30 nm is the thickness of the membrane, η_{pore} = 10.0 mPa·s, and η_0 = 1.002 mPa·s.[42,43] At the walls of the nanopore, the velocity was set to the boundary condition $v_\perp = \mu_{eo} E_\perp$, where the electric field $E = -\nabla V$ is determined from eq 1 and the electro-osmotic mobility is given by $\mu_{eo} = -\varepsilon\varepsilon_0\zeta/\eta$, where ζ is the zeta-potential. The Grahame equation[44]

$$\sigma(\zeta) = \sqrt{8 n_0 \varepsilon \varepsilon_0 k_B T}\, \sinh\left(\frac{e\zeta}{2k_B T}\right) \quad (3)$$

was used to calculate the relationship between the zeta-potential and the surface charge density. In eq 3, e is the elementary charge and $k_B T$ is the thermal energy at T = 298 K. The electrophoretic motion of ions of species i through the nanopore was calculated using the Nernst−Planck equation:

$$\nabla \cdot (n_i v) = D_i \nabla^2 n_i + z_i \mu_i c_i \nabla^2 V \quad (4)$$

where D_i is the diffusion coefficient and μ_i is the electrophoretic mobility of each ion. The diffusion coefficient and the mobility of each ion are $D_K = 1.33 \times 10^{-9}$ m^2 s^{-1} and $\mu_K = 7.6 \times 10^{-8}$ m^2 V^{-1} s^{-1} for potassium and $D_{Cl} = 2.03 \times 10^{-9}$ m^2 s^{-1} and $\mu_{Cl} = 7.9 \times 10^{-8}$ m^2 $V^{-1}s^{-1}$ for chlorine.[46] The transmembrane potential, V, in eq 4 was determined from eq 1, and the velocity, v, was determined from eq 2. To simulate translocations through the nanopore, DNA was treated as a point particle with a diffusion coefficient D = 1.57 μm^2 s^{-1} and mobility μ = 1.5 × 10^4 μm^2 V^{-1} s^{-1}.

Particle Tracking. Fluorescent image sequences of 20 kbp linear DNA and 8.6 kbp plasmids at 6.6 and 27 frames per second, respectively, were analyzed with ImageJ and the MTrackJ plugin, allowing for a semiautomatic particle tracking using the autosnap function which detects the particle's position by calculating the intensity-weighted mean position of pixels having a value above a certain threshold. The threshold, which is automatically computed, is the value that maximizes the interclass variance between objects and background pixels (Otsu's threshold).[47] Over 50 particles were traced for about 15 time-steps each.

Conflict of Interest: The authors declare no competing financial interest.

Acknowledgment. We gratefully acknowledge the contribution of circular plasmid DNA from T. Tanaka, and illuminating conversations with him and W. Timp. This work was funded by grants from the National Science Foundation (CCF 1129098 and DBI 1256052).

Supporting Information Available: 1. Two movies showing single molecules translocating through a pore. 2. Figure S1 showing particle tracking in the vicinity of the nanopore. 3. Figure S2 showing the *Z*-component of the electric field along the pore axis for pores ranging from 3.5 to 100 nm in diameter. 4. Figure S3 showing electric potential energy along the *z* axis in nanopores ranging from 3.5 to 100 nm in diameter in either 10 or 30 nm thick membranes. 5. Contour plots showing the electric potential energy above nanopores ranging from 3.5 to 100 nm in diameter as well as the capture radius above each pore. This material is available free of charge *via* the Internet at http://pubs.acs.org.

REFERENCES AND NOTES

1. Cherf, G. M.; Lieberman, K. R.; Rashid, H.; Lam, C. E.; Karplus, K.; Akeson, M. Automated Forward and Reverse Ratcheting of DNA in a Nanopore at 5-Å Precision. *Nat. Biotechnol.* **2012**, *30*, 344–348.
2. Manrao, E. A.; Derrington, I. M.; Laszlo, A. H.; Langford, K. W.; Hopper, M. K.; Gillgren, N.; Pavlenok, M.; Niederweis, M.; Gundlach, J. H. Reading DNA at Single-Nucleotide Resolution with a Mutant MspA Nanopore and Phi29 DNA Polymerase. *Nat. Biotechnol.* **2012**, *30*, 349–353.
3. Purnell, R. F.; Schmidt, J. J. Discrimination of Single Base Substitutions in a DNA Strand Immobilized in a Biological Nanopore. *ACS Nano* **2009**, *3*, 2533–2538.
4. Stoddart, D.; Heron, A. J.; Mikhailova, E.; Maglia, G.; Bayley, H. Single-Nucleotide Discrimination in Immobilized DNA Oligonucleotides with a Biological Nanopore. *Proc. Natl. Acad. Sci. U.S.A.* **2009**, *106*, 7702–7707.
5. Kasianowicz, J. J.; Brandin, E.; Branton, D.; Deamer, D. W. Characterization of Individual Polynucleotide Molecules Using a Membrane Channel. *Proc. Natl. Acad. Sci. U.S.A.* **1996**, *93*, 13770–13773.
6. Talaga, D. S.; Li, J. Single-Molecule Protein Unfolding in Solid State Nanopores. *J. Am. Chem. Soc.* **2009**, *131*, 9287–9297.
7. Yusko, E. C.; Johnson, J. M.; Majd, S.; Prangkio, P.; Rollings, R. C.; Li, J.; Yang, J.; Mayer, M. Controlling Protein Translocation through Nanopores with Bio-inspired Fluid Walls. *Nat. Nanotechnol.* **2011**, *6*, 253–260.
8. Wei, R.; Gatterdam, V.; Wieneke, R.; Tampe, R.; Rant, U. Stochastic Sensing of Proteins with Receptor-Modified Solid-State Nanopores. *Nat. Nanotechnol.* **2012**, *7*, 257–263.
9. Cressiot, B.; Oukhaled, A.; Patriarche, G.; Pastoriza-Gallego, M.; Betton, J.-M.; Auvray, L.; Muthukumar, M.; Bacri, L.; Pelta, J. Protein Transport through a Narrow Solid-State Nanopore at High Voltage: Experiments and Theory. *ACS Nano* **2012**, *6*, 6236–6243.
10. White, R. J.; Ervin, E. N.; Yang, T.; Chen, X.; Daniel, S.; Cremer, P. S.; White, H. S. Single Ion-Channel Recordings Using Glass Nanopore Membranes. *J. Am. Chem. Soc.* **2007**, *129*, 11766–11775.
11. Pierce, N. A.; Winfree, E. Protein Design Is NP-Hard. *Protein Eng.* **2002**, *15*, 779–782.
12. Li, Z.; Yang, Y.; Zhan, J.; Dai, L.; Zhou, Y. Energy Functions in *De Novo* Protein Design: Current Challenges and Future Prospects. *Annu. Rev. Biophys*, **2013**, DOI: 10.1146/annurev-biophys-083012-130315.
13. Aksimentiev, A.; Heng, J. B.; Timp, G.; Schulten, K. Microscopic Kinetics of DNA Translocation through Synthetic Nanopores. *Biophys. J.* **2004**, *87*, 2086–2097.
14. Chang, H.; Kosari, F.; Andreadakis, G.; Alam, M. A.; Vasmatzis, G.; Bashir, R. DNA-Mediated Fluctuations in Ionic Current through Silicon Oxide Nanopore Channels. *Nano Lett.* **2004**, *4*, 1551–1556.
15. Smeets, R. M. M.; Keyser, U. F.; Krapf, D.; Wu, M.-Y.; Dekker, N. H.; Dekker, C. Salt Dependence of Ion Transport and DNA Translocation through Solid-State Nanopores. *Nano Lett.* **2006**, *6*, 89–95.
16. Comer, J.; Dimitrov, V.; Zhao, Q.; Timp, G.; Aksimentiev, A. Microscopic Mechanics of Hairpin DNA Translocation through Synthetic Nanopores. *Biophys. J.* **2009**, *96*, 593–608.
17. van den Hout, M.; Krudde, V.; Janssen, X. J. A.; Dekker, N. H. Distinguishable Populations Report on the Interactions of Single DNA Molecules with Solid-State Nanopores. *Biophys. J.* **2010**, *99*, 3840–3848.
18. Wanunu, M.; Sutin, J.; McNally, B.; Chow, A.; Meller, A. DNA Translocation Governed by Interactions with Solid-State Nanopores. *Biophys. J.* **2008**, *95*, 4716–4725.
19. Movileanu, L.; Schmittschmitt, J. P.; Martin Scholtz, J.; Bayley, H. Interactions of Peptides with a Protein Pore. *Biophys. J.* **2005**, *89*, 1030–1045.
20. Wolfe, A. J.; Mohammad, M. M.; Cheley, S.; Bayley, H.; Movileanu, L. Catalyzing the Translocation of Polypeptides through Attractive Interactions. *J. Am. Chem. Soc.* **2007**, *129*, 14034–14041.
21. Heng, J. B.; Ho, C.; Kim, T.; Timp, R.; Aksimentiev, A.; Grinkova, Y. V.; Sligar, S.; Schulten, K.; Timp, G. Sizing DNA Using a Nanometer-Diameter Pore. *Biophys. J.* **2004**, *87*, 2905–2911.
22. Perry, J. M.; Zhou, K.; Harms, Z. D.; Jacobson, S. C. Ion Transport in Nanofluidic Funnels. *ACS Nano* **2010**, *4*, 3897–3902.
23. Ando, G.; Hyun, C.; Li, J.; Mitsui, T. Directly Observing the Motion of DNA Molecules near Solid-State Nanopores. *ACS Nano* **2012**, *6*, 10090–10097.
24. Heron, A. J.; Thompson, J. R.; Cronin, B.; Bayley, H.; Wallace, M. I. Simultaneous Measurement of Ionic Current and Fluorescence from Single Protein Pores. *J. Am. Chem. Soc.* **2009**, *131*, 1652–1653.
25. Soni, G. V.; Singer, A.; Yu, Z.; Sun, Y.; McNally, B.; Meller, A. Synchronous Optical and Electrical Detection of Biomolecules Traversing through Solid-State Nanopores. *Rev. Sci. Instrum.* **2010**, *81*, 014301.
26. Thacker, V. V.; Ghosal, S.; Hernández-Ainsa, S.; Bell, N. A.; Keyser, U. F. Studying DNA Translocation in Nanocapillaries Using Single Molecule Fluorescence. *Appl. Phys. Lett.* **2012**, *101*, 223704.
27. Song, W.; Pang, P.; He, J.; Lindsay, S. Optical and Electrical Detection of Single-Molecule Translocation through Carbon Nanotubes. *ACS Nano* **2013**, *7*, 689–694.
28. Wanunu, M.; Sutin, J.; Meller, A. DNA Profiling Using Solid-State Nanopores: Detection of DNA-Binding Molecules. *Nano Lett.* **2009**, *9*, 3498–3502.
29. Ho, C.; Qiao, R.; Heng, J. B.; Chatterjee, A.; Timp, R. J.; Aluru, N. R.; Timp, G. Electrolytic Transport through a Synthetic Nanometer-Diameter Pore. *Proc. Natl. Acad. Sci. U.S.A.* **2005**, *102*, 10445–10450.
30. Nelson, E. M.; Kurz, V.; Shim, J.; Timp, W.; Timp, G. Using a Nanopore for Single Molecule Detection and Single Cell Transfection. *Analyst* **2012**, *137*, 3020–3027.
31. Heng, J. B.; Aksimentiev, A.; Ho, C.; Marks, P.; Grinkova, Y. V.; Sligar, S.; Schulten, K.; Timp, G. The Electromechanics of DNA in a Synthetic Nanopore. *Biophys. J.* **2006**, *90*, 1098–1106.
32. Nakane, J.; Akeson, M.; Marziali, A. Evaluation of Nanopores as Candidates for Electronic Analyte Detection. *Electrophoresis* **2002**, *23*, 2592–2601.
33. Grosberg, A. Y.; Rabin, Y. DNA Capture into a Nanopore: Interplay of Diffusion and Electrohydrodynamics. *J. Chem. Phys.* **2010**, *133*, 165102.
34. Luan, B.; Aksimentiev, A. Electro-osmotic Screening of the DNA Charge in a Nanopore. *Phys. Rev. E* **2008**, *78*, 021912.
35. Araki, S.; Nakai, T.; Hizume, K.; Takeyasu, K.; Yoshikawa, K. Hydrodynamic Radius of Circular DNA Is Larger than That of Linear DNA. *Chem. Phys. Lett.* **2006**, *418*, 255–259.
36. Gurrieri, S.; Wells, K. S.; Johnson, I. D.; Bustamante, C. Direct Visualization of Individual DNA Molecules by Fluorescence Microscopy: Characterization of the Factors Affecting Signal/Background and Optimization of Imaging Conditions Using YOYO. *Anal. Biochem.* **1997**, *249*, 44–53.
37. Robertson, R. M.; Laib, S.; Smith, D. E. Diffusion of Isolated DNA Molecules: Dependence on Length and Topology. *Proc. Natl. Acad. Sci. U.S.A.* **2006**, *103*, 7310–7314.
38. Zhang, C.; Zhang, F.; van Kan, J. A.; van der Maarel, J. R. C. Effects of Electrostatic Screening on the Conformation of Single DNA Molecules Confined in a Nanochannel. *J. Chem. Phys.* **2008**, *128*, 225109.

39. Mirsaidov, U.; Comer, J.; Dimitrov, V.; Aleksei, A.; Timp, G. Slowing the Translocation of Double-Stranded DNA Using a Nanopore Smaller than the Double Helix. *Nanotechnology* **2010**, *21*, 395501.
40. Lederer, H.; May, R. P.; Kjems, J. K.; Baer, G.; Heumann, H. Solution Structure of a Short DNA Fragment Studied by Neutron Scattering. *Eur. J. Biochem.* **1986**, *161*, 191–196.
41. Brinkers, S.; Dietrich, H. R. C.; de Groote, F. H.; Young, I. T.; Rieger, B. The Persistence Length of Double Stranded DNA Determined Using Dark Field Tethered Particle Motion. *J. Chem. Phys.* **2009**, *130*, 215105.
42. Liu, Y.; Wang, Q.; Lu, L. Transport Properties and Distribution of Water Molecules Confined in Hydrophobic Nanopores and Nanoslits. *Langmuir* **2004**, *20*, 6921–6926.
43. Milischuk, A. A.; Ladanyi, B. M. Structure and Dynamics of Water Confined in Silica Nanopores. *J. Chem. Phys.* **2011**, *135*, 174709.
44. Grahame, D. C. The Electrical Double Layer and the Theory of Electrocapillarity. *Chem. Rev.* **1947**, *41*, 441–501.
45. Nair, P.; Alam, M. Performance Limits of Nanobiosensors. *Appl. Phys. Lett.* **2006**, *88*, 233120.
46. Lide, D. R. *CRC Handbook of Chemistry and Physics*, 88th ed.; CRC Press: Boca Raton, FL, 2008.
47. Meijering, E.; Dzyubachyk, O.; Smal, I. Methods for Cell and Particle Tracking. *Methods Enzymol.* **2012**, *504*, 183–200.